Diagnostic Study

INTERNATIONAL JOURNAL OF SURGERY

OPEN

# An unsupervised learning model based on CT radiomics features accurately predicts axillary lymph node metastasis in breast cancer patients: diagnostic study

Limeng Qu, MSc[a,c], Xilong Mei, MSc[b], Zixi Yi, BSc[d], Qiongyan Zou, PhD[a,c], Qin Zhou, PhD[a,c], Danhua Zhang, PhD[a,c], Meirong Zhou, PhD[a,c], Lei Pei, PhD[a,c], Qian Long, PhD[a,c], Jiahao Meng, MSc[a,c], Huashan Zhang, MSc[e], Qitong Chen, PhD[a,c,*], Wenjun Yi, PhD[a,c,*]

**Background:** The accuracy of traditional clinical methods for assessing the metastatic status of axillary lymph nodes (ALNs) is unsatisfactory. In this study, the authors propose the use of radiomic technology and three-dimensional (3D) visualization technology to develop an unsupervised learning model for predicting axillary lymph node metastasis in patients with breast cancer (BC), aiming to provide a new method for clinical axillary lymph node assessment in patients with this disease.

**Methods:** In this study, we retrospectively analyzed the data of 350 patients with invasive BC who underwent lung-enhanced computed tomography (CT) and axillary lymph node dissection surgery at the Department of Breast Surgery of the Second Xiangya Hospital of Central South University. The authors used 3D visualization technology to create a 3D atlas of ALNs and identified the region of interest for the lymph nodes. Radiomic features were subsequently extracted and selected, and a prediction model for ALNs was constructed using the K-means unsupervised algorithm. To validate the model, the authors prospectively collected data from 128 BC patients who were clinically evaluated as negative at our center.

**Results:** Using 3D visualization technology, we extracted and selected a total of 36 CT radiomics features. The unsupervised learning model categorized 1737 unlabeled lymph nodes into two groups, and the analysis of the radiomic features between these groups indicated potential differences in lymph node status. Further validation with 1397 labeled lymph nodes demonstrated that the model had good predictive ability for axillary lymph node status, with an area under the curve of 0.847 (0.825–0.869). Additionally, the model's excellent predictive performance was confirmed in the 128 axillary clinical assessment negative cohort (cN0) and the 350 clinical assessment positive (cN+) cohort, for which the correct classification rates were 86.72 and 87.43%, respectively, which were significantly greater than those of clinical assessment methods.

**Conclusions:** The authors created an unsupervised learning model that accurately predicts the status of ALNs. This approach offers a novel solution for the precise assessment of ALNs in patients with BC.

**Keywords:** axillary lymph node, breast cancer, CT radiomics, unsupervised learning model

## Introduction

Breast cancer (BC) has emerged as the most prevalent malignant tumor worldwide, overtaking lung cancer, and constitutes 11.7% of all cancer diagnoses[1–3]. Additionally, it ranks as the fifth most common cause of cancer-related mortality globally. The primary cause of death in patients with BC is tumor metastasis and recurrence, and axillary lymph node metastasis (ALNM) is an important risk factor[4–6]. Consequently, early assessment of axillary lymph nodes (ALNs) plays a crucial role in the diagnostic

[a]Department of General Surgery, The Second Xiangya Hospital, Central South University, [b]Department of Radiology, The Second Xiangya Hospital of Central South University, [c]Clinical Research Center For Breast Disease In Hunan Province, Changsha, [d]Central South University, Changsha, Hunan and [e]Urinary Surgery, Changsha Central Hospital, Changsha, Hunan, China

Sponsorships or competing interests that may be relevant to content are disclosed at the end of this article.

*Corresponding author. Address: Department of General Surgery, The Second Xiangya Hospital of Central South University, No. 139, Renmin Central Road, Changsha 410011, People's Republic of China. Tel.: +86 186 084 033 18. E-mail: yiwenjun@csu.edu.cn (W. Yi), and Tel.: +86 18684908633. E-mail: faithchen909@csu.edu.cn (Q. Chen).



International Journal of Surgery (2024) 110:5363–5373

Received 27 February 2024; Accepted 29 May 2024

Supplemental Digital Content is available for this article. Direct URL citations are provided in the HTML and PDF versions of this article on the journal's website, www.lww.com/international-journal-of-surgery.

Published online 7 June 2024

http://dx.doi.org/10.1097/JS9.0000000000001778

and therapeutic processes for BC patients[6–13]. However, conventional clinical evaluation methods are hindered by their subjective nature and reliance on the expertise and discretion of medical professionals[14].

Computer-aided diagnosis (CAD) technology has demonstrated considerable promise in enhancing the accuracy and precision of detecting ALNM[15–17]. By utilizing machine learning, deep learning, and image analysis techniques, CAD autonomously analyzes and interprets medical imaging data, thereby helping physicians diagnose diseases and assess prognoses. This technology potentially improves the efficiency and effectiveness of BC axillary management[18,19]. Radiomics, a crucial component of CAD, is an emerging field that integrates medical imaging and computer science. Clinical issues can be analyzed by segmenting regions of interest (ROIs) in conventional medical images for tumor identification and characterization and extracting various radiomic features[20–22]. By the analysis of BC patient images, radiomic methods can be used to help physicians identify features associated with ALNM and develop predictive models[23–28].

Recent radiomic-based prediction methods primarily rely on the primary lesion of BC to infer ALNM (Supplementary Table 1, Supplemental Digital Content 2, http://links.lww.com/JS9/C721). However, the inherent heterogeneity of tumors presents challenges, and few studies have predicted ALNM based on the lymph node lesion itself[29,30]. Challenges include difficulty in locating ALNs, low detection rates on conventional imaging methods, and establishing labels for metastatic lymph nodes, which are limiting factors for the advancement of this technique.

In a prior study, we implemented VitaWorks 3D visualization technology for ALN localization, marking the first application of this technology[31]. It provides a comprehensive and visual representation of the spatial location, size, and morphology of lymph nodes. The detection rate surpassed that of computed tomography (CT) and ultrasound, identifying lymph nodes as small as 2–3 mm in diameter[31,32]. Building on this, we developed a 3D atlas of ALNs in BC using VitaWorks technology, enhancing detection rates and reducing reliance on radiologists' subjective diagnostics, thereby minimizing manual errors and increasing localization objectivity and accuracy. To overcome the challenge of limited labeled data, we employed unsupervised learning models. These models are adept at analyzing data and uncovering inherent patterns, even without labeled data.

Therefore, in this study, we propose utilizing 3D visualization technology for ALN localization and an unsupervised learning approach to establish an ALNM prediction model for patients with partial ALNM. We anticipate that this study will provide a novel method for accurate ALN assessment and offer more precise diagnostic and treatment guidance for BC patients (Fig. 1).

## HIGHLIGHTS

- This retrospective study located 1737 unlabeled computed tomography lymph node images based on three-dimensional visualization and trained an unsupervised learning model to predict axillary lymph node metastasis.
- The unsupervised learning model was validated in 1397 supervised lymph nodes with an area under the curve value of up to 0.847 (0.825–0.869), a sensitivity of 80.70% and a specificity of 88.84%. Correct classification rate (CCR) of 86.72% was validated in a prospective cN0 cohort of 128 cases. The validated CCR was 87.43% in a 350-case retrospective cN+ cohort.

## Methods

### *Patient selection*

This retrospective study analyzed data from patients diagnosed with invasive BC admitted to the Department of Breast Surgery at the Second Xiangya Hospital of Central South University from January 2019 to March 2023. The inclusion criteria were as follows (1): underwent BC surgery at our hospital with postoperative pathology confirming invasive BC (2); underwent axillary lymph node dissection (ALND) at our hospital (3); completed a high-resolution, thin-section enhanced CT scan of the lung in our radiology department within 1 month before surgery; and (4) had complete clinicopathological data. The exclusion criteria for patients were as follows (1): had bilateral primary or metastatic BC (2); received neoadjuvant therapy (NAT) before surgery (3); had incomplete or poor-quality CT scans, flat scans only, or scans conducted externally; and (4) had distant metastatic lesions or concurrent other malignancies.

After rigorous screening, 313 patients were included. Additionally, 37 additional cases of invasive BC patients with postoperative pathology indicating total ALNM were collected from our center between January 2016 and March 2023; none of these patients underwent NAT or met the inclusion criteria. Furthermore, we prospectively collected data from 128 early-stage BC patients with negative axillary clinical evaluations between January and July 2023. These patients initially underwent sentinel lymph node biopsy (SLNB) surgery. If metastasis was detected in the sentinel lymph node (SLN) during intraoperative frozen section pathology, the patients underwent ALND surgery (Fig. 2).

Clinical pathology data extracted from the electronic medical records included patient factors such as age, menopausal status, pathological TNM stage, examination report time, tumor type, grade, estrogen receptor (ER) status, progesterone receptor (PR) status, human epidermal growth factor receptor 2 (HER2) status, the Ki-67 index, tumor molecular typing, the number of ALNMs, and total ALNs. The CT data included hospitalization number, CT number, and exam time. The study adhered to the Helsinki ethical statement standards and was approved by the Ethics Review Committee of Xiangya Second Hospital, Central South University, under the ethics number LYF2023043. The work has been reported in line with the Standards for the Reporting of Diagnostic accuracy studies (STARD) (Supplemental Digital Content 1, http://links.lww.com/JS9/C720) criteria[33].

### *CT image acquisition*

All recruited patients underwent high-resolution thin-section enhanced CT of the lungs within one month before surgery. The CT images were acquired using three machine models (1): GE Revolution 256 and GE 680 64 (2); Siemens Somatom Perspective, Siemens Somatom Definition Flash, and Siemens

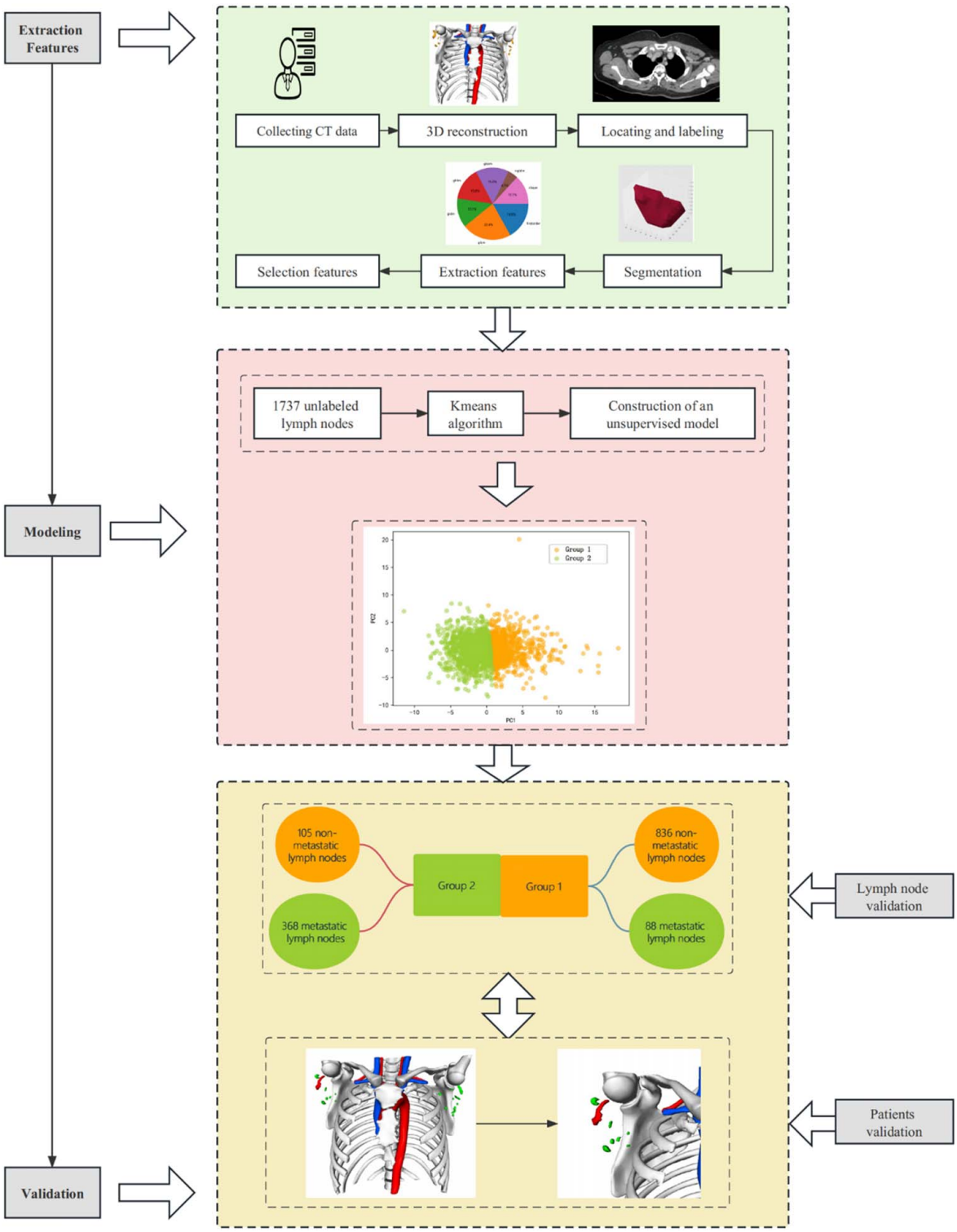


**Figure 1.** Schematic of the study design.

Somatom Force; and (3) United Imaging uCT780. For scanning, patients were placed in a supine position with their arms raised and aligned along the midline of the bed. The scans were extended from the lung apex to the lower edge of the twelfth thoracic vertebra using an orthostatic localization image. The CT parameters included a tube voltage of 120 kV, a tube current of 200 mAs, a frame rotation time of 0.5 s, and detector collimation of 64 mm × 0.625

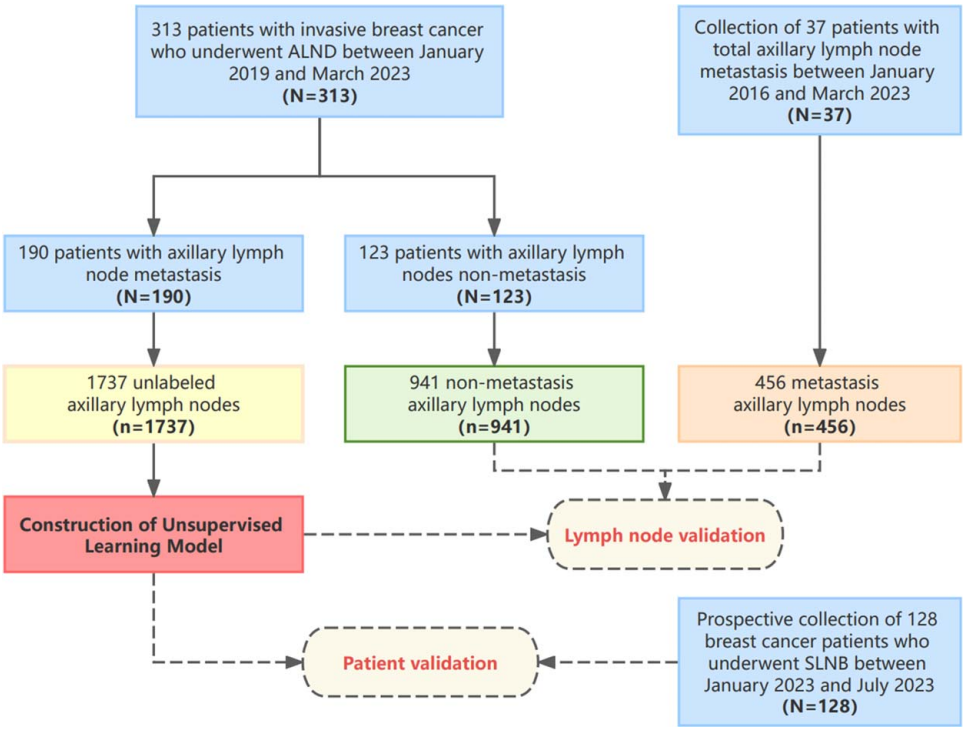


**Figure 2.** Overall flow chart of this study. ALND, axillary lymph node dissection; SLNB, sentinel lymph node biopsy.

mm. The field of view ranged from 400 to 500 mm, with a 512 × 512 matrix, a layer thickness of 1 mm, and zero layer spacing. The contrast agent, iopromide, was administered via the elbow vein using a dual-tube high-pressure syringe at a flow rate of 3.0 ml/s and a dosage of 1.2 ml/kg, followed by a 30 ml saline flush.

Radiologists transferred the raw CT data of patients onto CD-ROMs in DICOM format for storage. Lymph nodes identified in CT images were classified based on pathology reports: non-metastatic if all examined nodes were free of metastases and metastatic if pathology indicated metastasis in all examined nodes.

### 3D visualization technology

This study utilized 3D visualization technology developed by Shanghai Evision Medical Technology Co., Ltd., to reconstruct 3D images from 2D CT scans of each patient. The technology used algorithms for the automatic identification, segmentation, and extraction of ALN information and subsequently constructed a 3D ALN atlas. The 3D ALN atlas of each patient was viewed and manipulated using VitaWorks software (http://www.vitaworks.cn/), with the localization navigation function determining the position of the target lymph node on the CT image.

### Segmentation and labeling of the ROI of the ALN

Lymph node ROIs were segmented using the 3D-Slicer software segmentation module[34]. Since a lymph node appears across multiple CT image layers, segmentation was performed on each layer to fully capture the 3D structural features. The markers were subsequently applied to the 3D ALN atlas, establishing a one-to-one correspondence with the CT image lymph nodes.

### CT radiomic feature extraction and selection

The Radiomics module in 3D-Slicer software[34] was used to extract features from the ROI masks in the original CT images. Before extraction, the voxel size was resampled to $1 \times 1 \times 1$ mm$^3$, and the histogram width interval for image gray values was set at 25. From each target lymph node, 107 quantitative radiomic features across seven categories were extracted, and the Z scores were normalized. A correlation analysis then eliminated features with linear correlations exceeding 0.9, leaving 36 features with the highest predictive performance.

### Statistical analysis

The baseline data were analyzed using R Studio's R version 4.1.3 (R Project for Statistical Computing) and SPSS v27.0[35]. Normally distributed quantitative data are presented as the mean ± SD, while non-normally distributed data are presented as the median and interquartile range. Categorical data are summarized using frequencies and percentages. The normality of the quantitative data was assessed using the Shapiro—Wilk test (normal distribution considered at $P > 0.05$), and variance homogeneity was assessed using the Bartlett test (chi-square considered at $P > 0.05$). Unsupervised modeling and validation were performed with the K-means algorithm. The area under the curve (AUC) CIs were calculated using the Wilson interval scoring method. Significance levels were two-

**Table 1**

**Baseline characteristics of each cohort.**

| | Training set (*N* = 190) | Validation set (*N* = 160) | cN0 (*N* = 128) | cN + (*N* = 350) |
|---|---|---|---|---|
| Age | | | | |
| Mean (SD) | 51.6 (10.9) | 52.6 (10.6) | 52.7 (10.7) | 52.1 (10.8) |
| Median [Min, Max] | 51.5 [28.0, 79.0] | 52.0 [21.0, 81.0] | 53.0 [26.0, 79.0] | 52.0 [21.0, 81.0] |
| Pathological types | | | | |
| IDC | 185 (97.4%) | 150 (93.8%) | 121 (94.5%) | 334 (95.4%) |
| ILC | 3 (1.6%) | 8 (5.0%) | 5 (3.9%) | 11 (3.1%) |
| IMC | 1 (0.5%) | 1 (0.6%) | 1 (0.8%) | 3 (0.9%) |
| IMPC | 1 (0.5%) | 1 (0.6%) | 1 (0.8%) | 2 (0.6%) |
| Histological grade | | | | |
| I | 0 (0%) | 2 (1.3%) | 17 (13.3%) | 2 (0.6%) |
| II | 149 (78.4%) | 131 (81.9%) | 99 (77.3%) | 280 (80.0%) |
| III | 41 (21.6%) | 27 (16.9%) | 12 (9.4%) | 68 (19.4%) |
| T | | | | |
| T1 | 41 (21.6%) | 46 (28.8%) | 53 (41.4%) | 87 (24.9%) |
| T2 | 135 (71.1%) | 107 (66.9%) | 71 (55.5%) | 242 (69.1%) |
| T3 | 14 (7.4%) | 7 (4.4%) | 4 (3.1%) | 21 (6.0%) |
| N | | | | |
| N0 | 0 (0%) | 123 (76.9%) | 91 (71.1%) | 123 (35.1%) |
| N1 | 119 (62.6%) | 0 (0%) | 34 (26.6%) | 119 (34.0%) |
| N2 | 57 (30.0%) | 4 (2.5%) | 1 (0.8%) | 61 (17.4%) |
| N3 | 14 (7.4%) | 33 (20.6%) | 2 (1.6%) | 47 (13.4%) |
| Molecular subtype | | | | |
| HER2 + | 45 (23.7%) | 46 (28.8%) | 32 (25.0%) | 91 (26.0%) |
| Luminal-A | 23 (12.1%) | 28 (17.5%) | 43 (33.6%) | 51 (14.6%) |
| Luminal-B | 85 (44.7%) | 57 (35.6%) | 41 (32.0%) | 142 (40.6%) |
| TNBC | 37 (19.5%) | 29 (18.1%) | 12 (9.4%) | 66 (18.9%) |
| ER | | | | |
| Negative | 61 (32.1%) | 57 (35.6%) | 29 (22.7%) | 118 (33.7%) |
| Positive | 129 (67.9%) | 103 (64.4%) | 99 (77.3%) | 232 (66.3%) |
| PR | | | | |
| Negative | 73 (38.4%) | 70 (43.8%) | 42 (32.8%) | 143 (40.9%) |
| Positive | 117 (61.6%) | 90 (56.3%) | 86 (67.2%) | 207 (59.1%) |
| HER-2 | | | | |
| Negative | 145 (76.3%) | 114 (71.3%) | 96 (75.0%) | 259 (74.0%) |
| Positive | 45 (23.7%) | 46 (28.8%) | 32 (25.0%) | 91 (26.0%) |
| Ki-67 | | | | |
| < 14 | 25 (13.2%) | 37 (23.1%) | 50 (39.1%) | 62 (17.7%) |
| ≥ 14 | 165 (86.8%) | 123 (76.9%) | 78 (60.9%) | 288 (82.3% |

ER, estrogen receptor; HER-2, human epidermal growth factor receptor 2; IDC, invasive ductal carcinoma; ILC, invasive lobular carcinoma; IMC, invasive mucinous carcinoma; IMPC, invasive micropapillary carcinoma; PR, progesterone receptor; TNBC, triple-negative breast cancer

sided, with $P < 0.05$ considered indicative of statistical significance.

## Results

### *Construction of the unsupervised learning model in the training set*

This study harnessed the data of 190 patients with partial ALNM as a training set to investigate the association between CT imaging and the metastatic status of ALNs. We extracted radiomic features from the 1737 unlabeled lymph nodes of these patients. The median age of the individuals in the training cohort was 52 years (IQR, 28–79 years), and most of the patients were in stage T2 (71.1%), while a substantial number were in stage N1 (62.6%) (Table 1). Following feature selection, 36 critical CT radiomic features were identified. An unsupervised learning model was subsequently developed based on these features, categorizing the enrolled ALNs into two groups: Group 1, with 1073 lymph nodes; and Group 2, with 664 lymph nodes (Fig. 3A).

### *Differential radiomic characterization of group 1 and group 2*

Upon analyzing the radiomic shape features of the two groups, we observed that Group 1 exhibited a greater surface-to-volume ratio and shorter least axis length, suggesting flatter and more regular-shaped lymph nodes. In contrast, patients in Group 2 presented lower flatness and elongation and greater least axis length, indicative of more spherical and irregularly shaped lymph nodes. Additionally, Group 2 patients' gray-level co-occurrence matrix (GLCM) features, including higher inverted difference normalization (IDN), inverse difference

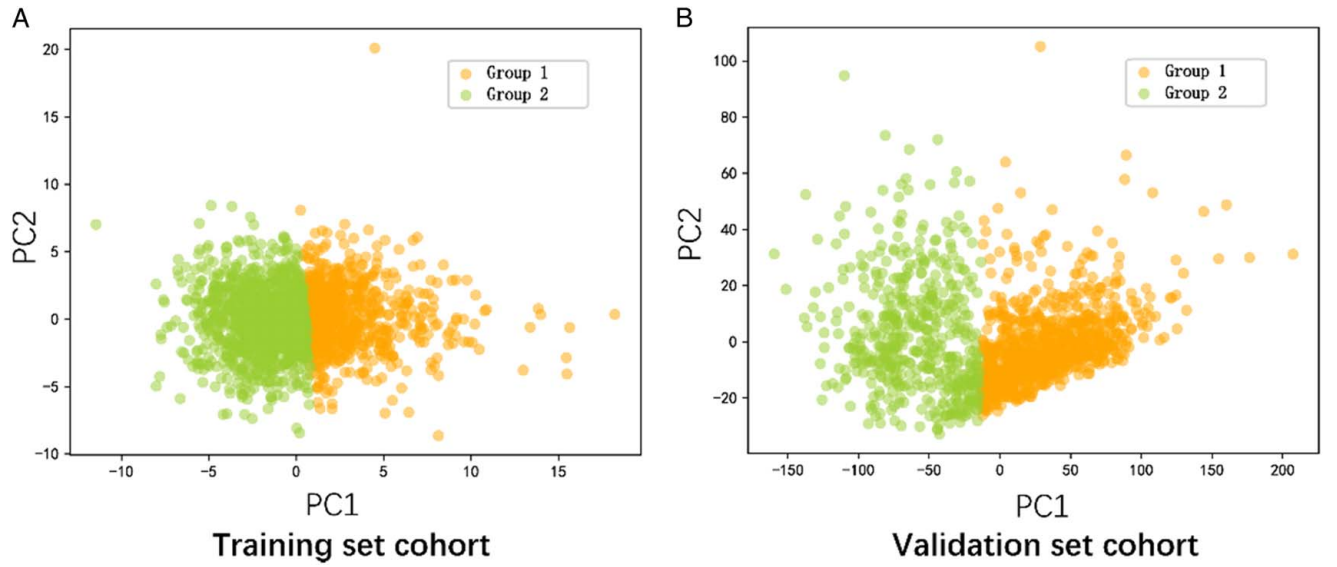


**Figure 3.** Clustering of ALNs in the training cohort (A) and validation cohort (B).

moment (IDM), and correlation, pointed to more complex textural characteristics. These observations led to the hypothesis that Group 2 might predominantly represent diseased ALNs (Fig. 4).

### *Lymph node-level validation in the validation set*

The validation cohort included 123 patients without ALN metastasis and 37 with complete lymph node metastasis, encompassing 941 nonmetastatic and 456 metastatic lymph nodes (Table 1). Using the unsupervised algorithm, these 1397 lymph nodes were divided into two groups (Group 1 and Group 2; Fig. 3B). Group 1 included 924 lymph nodes, 90.48% of which were nonmetastatic, whereas Group 2 included 473 lymph nodes, 77.80% of which were metastatic (Fig. 5A–B). The model's effectiveness was further corroborated by an AUC of 0.847 (95% CI: 0.825–0.869), a correct classification rate (CCR) of 86.18%, a sensitivity of 80.70%, and a specificity of 88.84%. These results confirmed the close relationship between the CT radiomic features and ALN status, demonstrating the superior predictive capability of the model (Fig. 5C-D).

### *Patient-level validation of the unsupervised model*

For external validation, we prospectively collected data from 128 clinical assessment negative (cN0) patients. Of these patients, 38 underwent ALND surgery due to intraoperative SLN metastasis. The model successfully predicted metastasis in 28 of these patients. Among the 90 patients without SLN metastasis, the model accurately predicted 83 patients. Hence, the model achieved a CCR of 86.72%, significantly surpassing the clinical assessment rate of 70.31% ($P < 0.001$; Fig. 6A, C; Table 2).

Additionally, validation was performed on 350 clinical assessment positive (cN+) patients. The model correctly identified lymph node metastasis in 216 out of 227 patients and accurately predicted the absence of metastasis in 90 out of 123 patients. The CCR for this model was 87.43%, which was markedly greater than the clinical assessment rate of 64.86% ($P < 0.001$; Fig. 6B, D; Table 3). Thus, the efficacy of the unsupervised model employing CT radiomic features as a predictor of ALNM in BC patients was demonstrated.

## Discussion

In this study, we utilized 3D visualization and radiomics techniques to extract a multitude of radiomic features from CT images of the ALNs. Utilizing the K-means unsupervised algorithm for predictive modeling in a subset of patients with partial ALNM (comprising 1737 unlabeled lymph nodes), we discovered a robust correlation between these radiomic features and the metastatic status of the ALNs in BC patients. Subsequent lymph node-level validation was performed on a total of 1397 labeled lymph nodes, encompassing both metastatic and nonmetastatic patients. Additionally, patient-level validation was conducted for 128 cN0 and 350 cN+ patients. The results demonstrated that our model significantly outperformed traditional clinical assessment methods in predicting ALNM, demonstrating remarkable predictive accuracy.

ALNM status critically impacts the prognosis of BC patients, necessitating the identification of those at intermediate to high-risk for tailored preoperative treatment[36,37]. Clinically, distinguishing metastatic from normal lymph nodes in BC patients is challenging using conventional methods[13,38–40]. For instance, Tan *et al.*[41] reported that their model, which incorporates clinicopathologic features, achieved an AUC of 81.9%, which was slightly reduced to 81% upon the inclusion of these features; Song *et al.*[42] extracted radiomic features from dynamic contrast-enhanced magnetic resonance imaging (DCE-MRI) to develop a predictive model, achieving an AUC of 80.5% in the validation

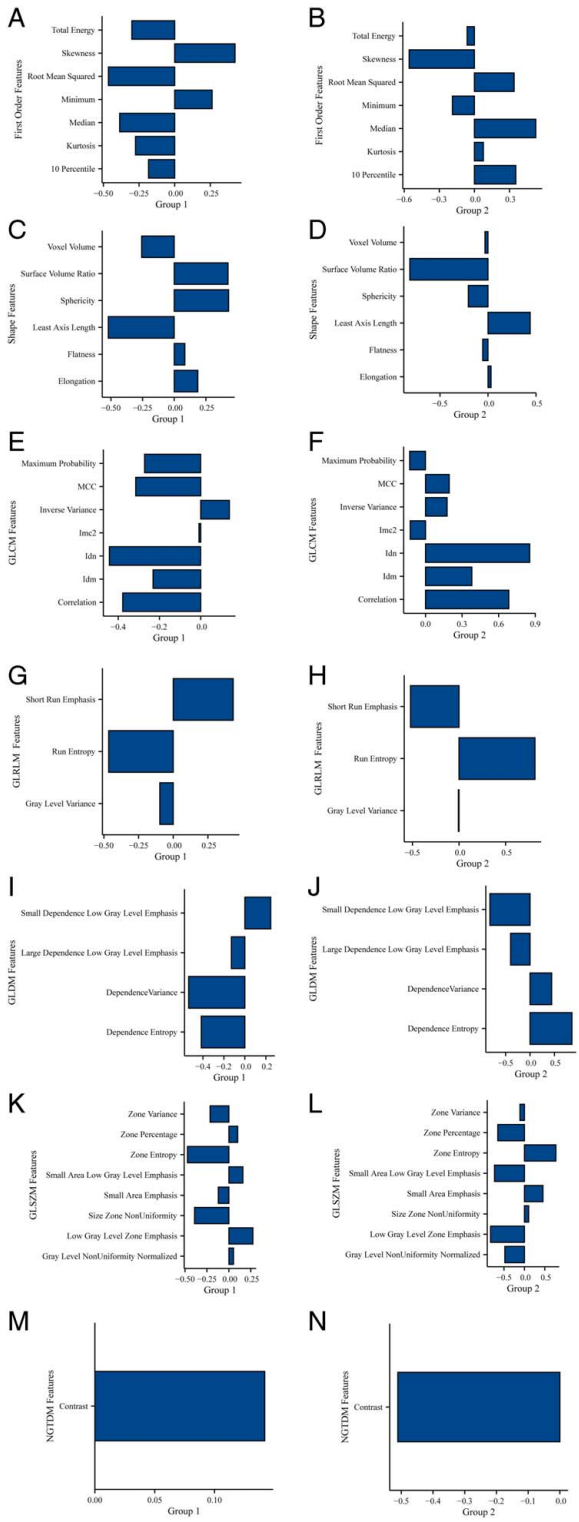


**Figure 4.** Radiomic characterization of Group 1 and Group 2. GLCM, gray level co-occurrence matrix; GLRLM, gray level run length matrix; GLDM, gray level dependence matrix, GLSZM, gray level size zone matrix; IMC2, informational measure of correlation 2; IDN, inverted difference normalization; IDM, inverse difference moment; MCC, maximum correlation coefficient; NGTDM, neighboring gray tone difference matrix.

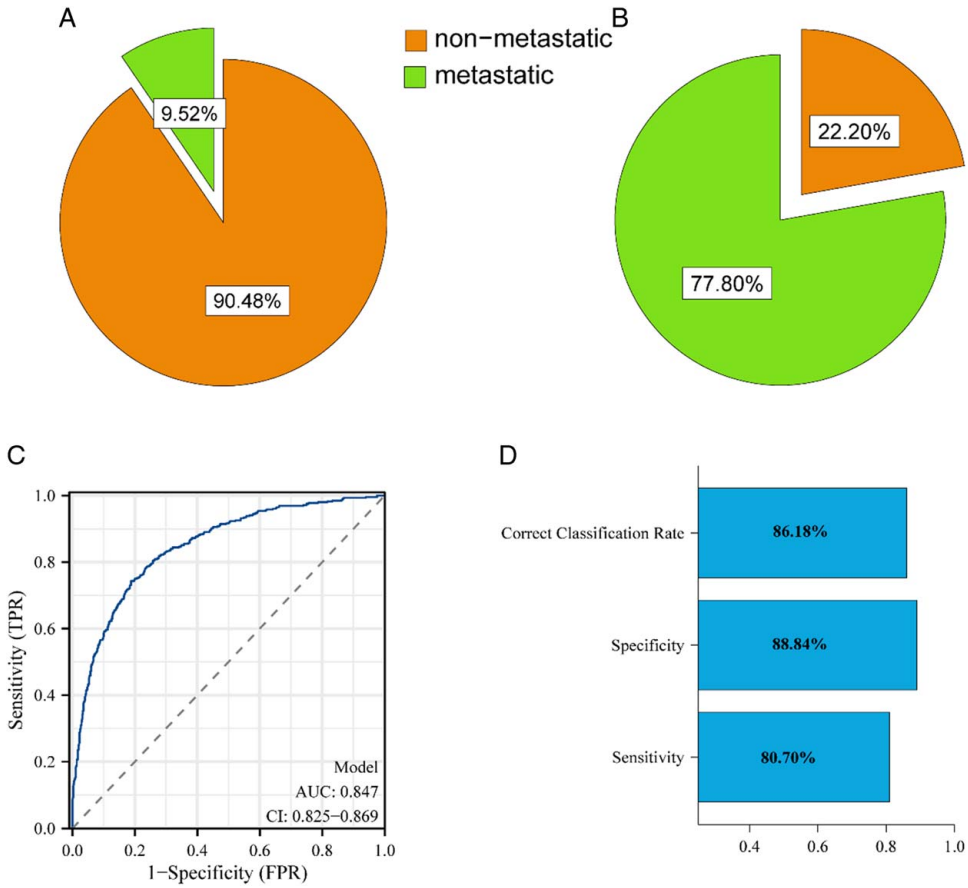


**Figure 5.** Validation of the unsupervised model at the lymph node level in the validation cohort A-B) Group 1 and Group 2 lymph node distributions; C) ROC curves of the unsupervised model; D) correct classification rate, specificity and sensitivity of the unsupervised model.

set, which increased to 86.7% with the integration of clinicopathologic factors into a nomogram. Additionally, Romeo *et al*.[43] developed a classifier based on 18F-FDG PET/MRI radiomics features from primary BC lesions, which exhibited an accuracy of 78.6% (AUC = 0.839) and a sensitivity and specificity of 67.9 and 100%, respectively, in the test set. Wang *et al*.[44] discovered that DCE-MRI-based radiomic models, both intratumoral and peritumoral, combined with clinico-radiological characteristics could predict ALN metastasis in BC patients with an AUC of up to 83.9%, indicating significant clinical applicability. Nevertheless, these methodologies are primarily focused on breast lesions (Supplementary Table 1, Supplemental Digital Content 2, http://links.lww.com/JS9/C721).

In our study, we adopted an unsupervised learning algorithm to analyze the morphological and textural characteristics of individual lymph nodes, among other features. This approach led to the identification of two distinct clusters, enabling effective categorization of ALNs based on radiomic features. Validation on 1397 labeled ALNs revealed an AUC of 0.847, with a specificity reaching 90.5%. These findings are pivotal for the diagnosis and treatment of ALNM in BC patients, helping clinicians develop a more accurate basis for decision-making. It also represents the first instance of an unsupervised learning prediction method that combines 3D visualization technology and CT-LN radiomic features, achieving innovations in both lymph node localization and characterization. In clinical applications involving cN0 and cN+ patients, the model achieved CRRs of 86.72 and 87.43%, respectively. These results indicate that the model not only accurately evaluates lymph nodes but also reliably identifies the presence of ALNM in patients. Notably, this model identified 28 high-risk patients among 128 cN0 individuals, aiding in the formulation of precise preoperative treatment strategies (Table 2). Similarly, 90 relatively low-risk patients were identified among the 350 cN+ individuals, potentially predicting unnecessary ALND (Table 3). Thus, this study introduces an efficacious approach for ALN resection prediction, showing considerable promise for clinical application.

Furthermore, the model we developed for predicting ALN status using CT radiomic features is straightforward, objective, cost effective, and free from subjective biases, leading to high diagnostic efficacy. The first ALNM prediction model was constructed based on CT images of individual lymph nodes. This study is not without limitations. First, it is based on retrospective data from a single-center clinical study. Therefore, further validation in a larger population from external medical institutions is needed. Second, the identification of lymph nodes using 3D visualization technology is contingent upon image contrast, which can be challenging when lymph nodes are near soft tissues. Finally, the false

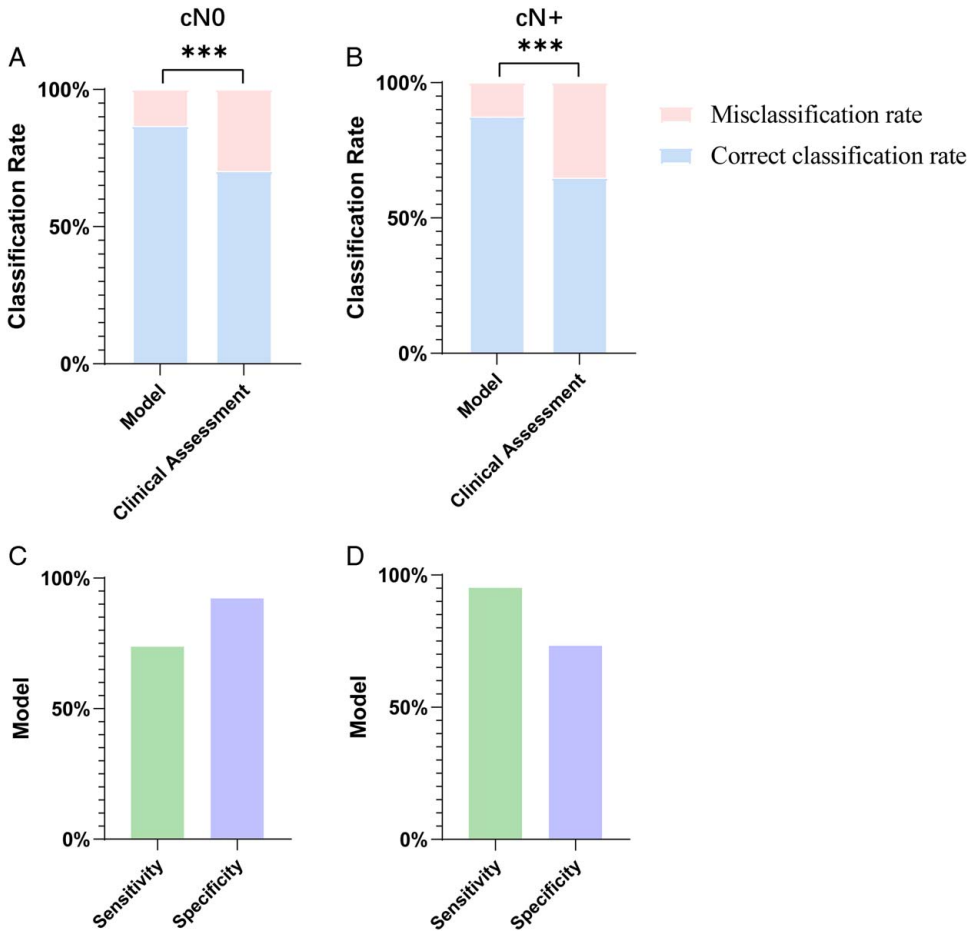


**Figure 6.** Assessment of unsupervised modeling in cN0 patients and cN + patients (A and C) correct classification and misclassification rates (A) and sensitivity and specificity (C) of the model for cN0 patients; (B and D) correct classification and misclassification rates (B) and sensitivity and specificity (D) of the model for cN + patients.

negative rate (FNR) of the model was higher than that of conventional SLNB in cN0 patients, which might cause patients to miss the best treatment opportunity; therefore, validation in larger samples and at external centers is needed before extending the model to the clinic. In addition, in future studies, we will carefully evaluate the difference between micrometastases and macrometastases, which is a key direction for follow-up studies. Despite these limitations, this study introduces a novel approach to the clinical assessment of ALNs, markedly enhancing the detection of metastatic lymph nodes and enabling the evaluation of residual ALNs post-surgery. This methodology has substantial potential for broad clinical adoption. Future research will focus on validating the reliability of the method.

In conclusion, this study presents a novel methodology for clinicians in the assessment of ALNM that could substantially influence decision-making regarding ALN surgery. Its implementation has the potential to markedly advance the field of individualized and precise diagnosis and treatment of metastatic disease in ALNs.

**Table 2**

**The assessment metrics of the model for cN0 patients.**

| | Pathological examination | | | | | | | |
|---|---|---|---|---|---|---|---|---|
| | Metastasis | No metastasis | Total | CCR | Sensitivity | Specificity | FPR | FNR |
| Model | | | | | | | | |
| Metastasis | 28 | 7 | 35 | 86.72% | 73.68% | 92.22% | 7.78% | 26.32% |
| No metastasis | 10 | 83 | 93 | | | | | |
| Total | 38 | 90 | 128 | | | | | |

CCR, correct classification rate; cN0, axillary clinical assessment negative; FNR, false negative rate; FPR, false positive rate.

**Table 3**

**The assessment metrics of the model for cN + patients.**

| | Pathological examination | | | | | | | |
|---|---|---|---|---|---|---|---|---|
| | Metastasis | No metastasis | Total | CCR | Sensitivity | Specificity | FPR | FNR |
| Model | | | | | | | | |
| Metastasis | 216 | 33 | 249 | 87.43% | 95.15% | 73.17% | 26.83% | 4.85% |
| No metastasis | 11 | 90 | 101 | | | | | |
| Total | 227 | 123 | 350 | | | | | |

CCR, correct classification rate; cN + , axillary clinical assessment positive; FNR, false negative rate; FPR, false positive rate.

## Ethical approval

The study adhered to the Helsinki ethical statement standards and was approved by the Ethics Review Committee of Xiangya Second Hospital, Central South University, under the ethics number LYF2023043.

## Consent

Not applicable.


## Source of funding

This study was funded by the science and technology innovation Program of Hunan Province (Grant No. 2021SK2026) and the Innovation Platform and Talent Plan of Hunan Province (2023SK4019).


## Author contribution

L.Q.: conceptualization, data curation, formal analysis, investigation, methodology, validation, visualization, writing – original draft, and writing – review and editing; X.M.: data curation, resources, supervision, and writing – review and editing; Z.Y.: data curation and formal analysis; Q.Z., Q.Z., D.Z., M.Z., L.P., Q.L., J.M., and H.Z.: data curation, investigation, and validation; Q.C.: conceptualization, methodology, supervision, writing – original draft, and writing – review and editing; W.Y.: conceptualization, formal analysis, funding acquisition, methodology, project administration, resources, supervision, and writing – review and editing.

## Conflicts of interest disclosure

All authors declare that they have no financial or other competing interests.

## Research registration unique identifying number (UIN)

We have registered on the https://www.isrctn.com/ISRCTN54288903. Unique Identifying Number (UIN): ISRCTN54288903.

## Guarantor

Wenjun Yi.

## Data availability statement

The datasets used and analyzed during the current study available from the corresponding author on reasonable request.

## Provenance and peer review

Not commissioned, externally peer-reviewed.


## Acknowledgements

Thanks to the anonymous peer-reviewers for their insightful suggestions and careful reading of the manuscript.


## References


[1] Ferlay J, Colombet M, Soerjomataram I, *et al*. Estimating the global cancer incidence and mortality in 2018: GLOBOCAN sources and methods. Int J Cancer 2019;144:1941–53.

[2] Sung H, Rosenberg PS, Chen W-Q, *et al*. Female breast cancer incidence among Asian and Western populations: more similar than expected. J Natl Cancer Inst 2015;107:djv107.

[3] Sung H, Ferlay J, Siegel RL, *et al*. Global Cancer Statistics 2020: GLOBOCAN estimates of incidence and mortality worldwide for 36 cancers in 185 countries. CA Cancer J Clin 2021;71:209–49.

[4] DeSantis CE, Ma J, Gaudet MM, *et al*. Breast cancer statistics, 2019. CA Cancer J Clin 2019;69:438–51.

[5] Siegel RL, Miller KD, Jemal A. Cancer Statistics, 2017. CA Cancer J Clin 2017;67:7–30.

[6] Giuliano AE, Kirgan DM, Guenther JM, *et al*. Lymphatic mapping and sentinel lymphadenectomy for breast cancer. Ann Surg 1994;220: 391–401.

[7] Galimberti V, Cole BF, Zurrida S, *et al*. Axillary dissection versus no axillary dissection in patients with sentinel-node micrometastases (IBCSG 23-01): a phase 3 randomised controlled trial. Lancet Oncol 2013;14: 297–305.

[8] Galimberti V, Cole BF, Viale G, *et al*. Axillary dissection versus no axillary dissection in patients with breast cancer and sentinel-node micrometastases (IBCSG 23-01): 10-year follow-up of a randomised, controlled phase 3 trial. Lancet Oncol 2018;19:1385–93.

[9] Lyman GH, Giuliano AE, Somerfield MR, *et al*. American Society of Clinical Oncology guideline recommendations for sentinel lymph node biopsy in early-stage breast cancer. J Clin Oncol 2005;23:7703–20.

[10] Krag DN, Anderson SJ, Julian TB, *et al*. Sentinel-lymph-node resection compared with conventional axillary-lymph-node dissection in clinically node-negative patients with breast cancer: overall survival findings from the NSABP B-32 randomised phase 3 trial. Lancet Oncol 2010;11: 927–33.

[11] Donker M, van Tienhoven G, Straver ME, *et al*. Radiotherapy or surgery of the axilla after a positive sentinel node in breast cancer (EORTC 10981-22023 AMAROS): a randomised, multicentre, open-label, phase 3 non-inferiority trial. Lancet Oncol 2014;15:1303–10.

[12] Giuliano AE, Ballman KV, McCall L, *et al*. Effect of axillary dissection vs no axillary dissection on 10-year overall survival among women with invasive breast cancer and sentinel node metastasis: the ACOSOG Z0011 (Alliance) randomized clinical trial. JAMA 2017;318:918–26.

[13] Heidinger M, Knauer M, Tausch C, *et al*. Tailored axillary surgery - A novel concept for clinically node positive breast cancer. Breast 2023;69: 281–9.
[14] Marino MA, Avendano D, Zapata P, *et al*. Lymph node imaging in patients with primary breast cancer: concurrent diagnostic tools. Oncologist 2020;25:e231–42.
[15] Zhou L-Q, Wu X-L, Huang S-Y, *et al*. Lymph node metastasis prediction from primary breast cancer US images using deep learning. Radiology 2020;294:19–28.
[16] Zheng X, Yao Z, Huang Y, *et al*. Deep learning radiomics can predict axillary lymph node status in early-stage breast cancer. Nat Commun 2020;11:1236.
[17] Moon WK, Lee Y-W, Huang Y-S, *et al*. Computer-aided prediction of axillary lymph node status in breast cancer using tumor surrounding tissue features in ultrasound images. Comput Methods Programs Biomed 2017;146:143–50.
[18] Moon WK, Chen IL, Yi A, *et al*. Computer-aided prediction model for axillary lymph node metastasis in breast cancer using tumor morphological and textural features on ultrasound. Comput Methods Programs Biomed 2018;162:129–37.
[19] Chmielewski A, Dufort P, Scaranelo AM. A computerized system to assess axillary lymph node malignancy from sonographic images. Ultrasound Med Biol 2015;41:2690–9.
[20] Mayerhoefer ME, Materka A, Langs G, *et al*. Introduction to radiomics. J Nucl Med 2020;61:488–95.
[21] Conti A, Duggento A, Indovina I, *et al*. Radiomics in breast cancer classification and prediction. Semin Cancer Biol 2021;72:238–50.
[22] Guiot J, Vaidyanathan A, Deprez L, *et al*. A review in radiomics: making personalized medicine a reality via routine imaging. Med Res Rev 2022; 42:426–40.
[23] Yu Y, Tan Y, Xie C, *et al*. Development and validation of a preoperative magnetic resonance imaging radiomics-based signature to predict axillary lymph node metastasis and disease-free survival in patients with early-stage breast cancer. JAMA Netw Open 2020;3:e2028086.
[24] Yu Y, He Z, Ouyang J, *et al*. Magnetic resonance imaging radiomics predicts preoperative axillary lymph node metastasis to support surgical decisions and is associated with tumor microenvironment in invasive breast cancer: a machine learning, multicenter study. EBioMedicine 2021;69:103460.
[25] Zhu Y, Ma Y, Zhang Y, *et al*. Radiomics nomogram for predicting axillary lymph node metastasis-a potential method to address the limitation of axilla coverage in cone-beam breast CT: a bi-center retrospective study. Radiol Med 2023;128:1472–82.
[26] Gu J, Tong T, Xu D, *et al*. Deep learning radiomics of ultrasonography for comprehensively predicting tumor and axillary lymph node status after neoadjuvant chemotherapy in breast cancer patients: a multicenter study. Cancer 2023;129:356–66.
[27] Zhu T, Huang Y-H, Li W, *et al*. Multifactor artificial intelligence model assists axillary lymph node surgery in breast cancer after neoadjuvant chemotherapy: multicenter retrospective cohort study. Int J Surg 2023; 109:3383–94.
[28] Wang Z, Zhang H, Lin F, *et al*. Intra- and peritumoral radiomics of contrast-enhanced mammography predicts axillary lymph node metastasis in patients with breast cancer: a multicenter study. Acad Radiol 2023;30(Suppl 2):S133–42.
[29] Song B-I. A machine learning-based radiomics model for the prediction of axillary lymph-node metastasis in breast cancer. Breast Cancer 2021;28: 664–71.
[30] Calabrese A, Santucci D, Landi R, *et al*. Radiomics MRI for lymph node status prediction in breast cancer patients: the state of art. J Cancer Res Clin Oncol 2021;147:1587–97.
[31] Qu L, Chen Q, Luo N, *et al*. 3D reconstruction based novel methods are more effective than traditional clinical assessment in breast cancer axillary lymph node metastasis prediction. Sci Rep 2022;12: 12425.
[32] Zhao P, Zou Q, Yuan L, *et al*. Application of a three-dimensional reconstruction system in breast cancer with ipsilateral supraclavicular lymph node metastasis: a case series. Breast Care (Basel) 2019;14: 176–9.
[33] Bossuyt, Reitsma PM, Bruns DE JB, *et al*. STARD 2015: an updated list of essential items for reporting diagnostic accuracy studies. BMJ 2015;351: h5527.
[34] Bruns N. 3D Slicer : Universal 3D visualization software. Unfallchirurg 2019;122:662–3.
[35] Dessau RB, Pipper CB. "R"--project for statistical computing. Ugeskr Laeger 2008;170:328–30.
[36] Rao R, Euhus D, Mayo HG, *et al*. Axillary node interventions in breast cancer: a systematic review. JAMA 2013;310:1385–94.
[37] Bundred NJ, Barnes NLP, Rutgers E, *et al*. Is axillary lymph node clearance required in node-positive breast cancer? Nat Rev Clin Oncol 2015;12:55–61.
[38] Chang JM, Leung JWT, Moy L, *et al*. Axillary nodal evaluation in breast cancer: state of the art. Radiology 2020;295:500–15.
[39] Jiang W, Meng R, Cheng Y, *et al*. Intra- and peritumoral based radiomics for assessment of lymphovascular invasion in invasive breast cancer. J Magn Reson Imaging 2023;59:613–25.
[40] Gao Y, Luo Y, Zhao C, *et al*. Nomogram based on radiomics analysis of primary breast cancer ultrasound images: prediction of axillary lymph node tumor burden in patients. Eur Radiol 2021;31:928–37.
[41] Tan H, Gan F, Wu Y, *et al*. Preoperative prediction of axillary lymph node metastasis in breast carcinoma using radiomics features based on the fat-suppressed T2 sequence. Acad Radiol 2020;27:1217–25.
[42] Song D, Yang F, Zhang Y, *et al*. Dynamic contrast-enhanced MRI radiomics nomogram for predicting axillary lymph node metastasis in breast cancer. Cancer Imaging 2022;22:17.
[43] Romeo V, Kapetas P, Clauser P, *et al*. Simultaneous 18F-FDG PET/MRI radiomics and machine learning analysis of the primary breast tumor for the preoperative prediction of axillary lymph node status in breast cancer. Cancers (Basel) 2023;15:5088.
[44] Wang Y, Shang Y, Guo Y, *et al*. Clinical study on the prediction of ALN metastasis based on intratumoral and peritumoral DCE-MRI radiomics and clinico-radiological characteristics in breast cancer. Front Oncol 2024;14:1357145.